

# Revealing the intricate dune-dune interactions of bidisperse barchans

Willian Righi Assis<sup>1,1</sup>, Fernando David Cúñez<sup>2,2</sup>, and Erick Franklin<sup>1,1</sup>

<sup>1</sup>UNICAMP - University of Campinas

<sup>2</sup>University of Rochester

November 30, 2022

## Abstract

Three dimensional dunes of crescentic shape, called barchans, are commonly found on Earth and other planetary environments. In the great majority of cases, barchans are organized in large fields in which corridors of size-selected barchans are observed, and where barchan-barchan interactions play an important role in size regulation. Previous studies shed light on the interactions between barchans by making use of monodisperse particles, but dunes in nature consist, however, of polydisperse grains. In this paper, we investigate the binary interactions of barchans consisting of (i) bidisperse mixtures of grains and (ii) different monodisperse grains (one type for each barchan). We performed experiments in a water channel where grains of different sizes were poured inside forming two barchans that interacted with each other while filmed by a camera, and we obtained their morphology from image processing. We observed that a transient stripe appears over the dunes in cases of bidisperse mixtures, that interaction patterns vary with concentrations, and that different interactions exist when each barchan consists of different monodisperse grains. Interestingly, we found the conditions for a collision in which the upstream barchan is larger than the downstream one, and we propose a timescale for the interactions of both monodisperse and bidisperse barchans. Our results represent a new step toward understanding complex barchanoid structures found on Earth, Mars and other celestial bodies.

# Revealing the intricate dune-dune interactions of bidisperse barchans

An edited version of this paper was published by AGU. Copyright (2021) American Geophysical Union. Assis, W. R., Cúñez, F. D. and Franklin, E. M. (2022). Revealing the intricate dune-dune interactions of bidisperse barchans. *Journal of Geophysical Research: Earth Surface*, 127, e2021JF006588. <https://doi.org/10.1029/2021JF006588>  
To view the published open abstract, go to <https://doi.org/10.1029/2021JF006588>.

W. R. Assis<sup>1</sup>, F. D. Cúñez<sup>2</sup>, E. M. Franklin<sup>1</sup>

<sup>1</sup>School of Mechanical Engineering, UNICAMP - University of Campinas, Rua Mendeleev, 200, Campinas, SP, Brazil

<sup>2</sup>Department of Earth and Environmental Sciences, University of Rochester, Rochester, NY 14627, USA

## Key Points:

- Two-species barchan-barchan interactions vary with the relative concentrations of each species
- We found configurations distinct from the one-species case, including a collision in which the upstream barchan is the largest
- We propose a timescale for the interactions of both monodisperse and bidisperse barchans

---

Corresponding author: Erick M. Franklin, [erick.franklin@unicamp.br](mailto:erick.franklin@unicamp.br)

**Abstract**

Three dimensional dunes of crescentic shape, called barchans, are commonly found on Earth and other planetary environments. In the great majority of cases, barchans are organized in large fields in which corridors of size-selected barchans are observed, and where barchan-barchan interactions play an important role in size regulation. Previous studies shed light on the interactions between barchans by making use of monodisperse particles, but dunes in nature consist, however, of polydisperse grains. In this paper, we investigate the binary interactions of barchans consisting of (i) bidisperse mixtures of grains and (ii) different monodisperse grains (one type for each barchan). We performed experiments in a water channel where grains of different sizes were poured inside forming two barchans that interacted with each other while filmed by a camera, and we obtained their morphology from image processing. We observed that a transient stripe appears over the dunes in cases of bidisperse mixtures, that interaction patterns vary with concentrations, and that different interactions exist when each barchan consists of different monodisperse grains. Interestingly, we found the conditions for a collision in which the upstream barchan is larger than the downstream one, and we propose a timescale for the interactions of both monodisperse and bidisperse barchans. Our results represent a new step toward understanding complex barchanoid structures found on Earth, Mars and other celestial bodies.

**Plain Language Summary**

Barchans are crescent-shaped dunes commonly found in dune fields on Earth and other planetary environments, and it has been shown that their sizes are highly influenced by barchan-barchan interactions. The composition of the granular bed can affect the observed patterns and sizes, but had not been investigated until now. Because those interactions take long times to be completed in gaseous environments (estimated in decades and millennia for dunes on terrestrial and Martian deserts, respectively) when compared with the aquatic case (of the order of minutes), we performed experiments in a water channel where two species of grains (in terms of size) were poured inside, forming two barchans that interacted with each other. We found different structures, including a collision in which the upstream barchan is the largest, and propose a timescale for the interactions of barchans. The identification of such timescale represents a new step for predicting the duration of barchan-barchan interactions and, more generally, scaling the evolution of dune fields on Earth, Mars and other planetary environments.

**1 Introduction**

Under one-directional fluid flow and limited amount of sand, three dimensional dunes of crescentic shape, called barchans, consistently grow (Bagnold, 1941; Herrmann & Sauer-  
mann, 2000; Hersen, 2004), being commonly found on Earth, Mars, other celestial bodies (Elbelrhiti et al., 2005; Claudin & Andreotti, 2006; E. J. R. Parteli & Herrmann, 2007). In the great majority of cases, barchans are organized in large fields in which corridors of size-selected barchans are observed, and where barchan-barchan interactions play an important role in size regulation (Hersen et al., 2004; Hersen & Douady, 2005; Kocurek et al., 2010; Génois, Hersen, et al., 2013; Génois, du Pont, et al., 2013; Assis & Franklin, 2020, 2021). Given the ubiquitous nature of barchans, understanding how their shape is formed, how they self-organize in regular fields, and how they are affected by the bed granulometry are of paramount importance to deduce the past and predict the future of barchans on Earth and other planetary environments.

Several studies investigated the interactions between barchans, shedding light on certain aspects of barchan-barchan interactions, but leaving many others, however, poorly understood. One of the drawbacks of previous studies is that field measurements were very limited in time, since aeolian barchans take decades to interact completely with each

69 other (Bagnold, 1941; Hersen et al., 2002). Field measurements of aeolian barchan-barchan  
70 interactions are of course important, since they measure processes happening in nature,  
71 and previous studies showed that the collisions of barchans regulate their size and gen-  
72 erate different barchanoid forms (Norris & Norris, 1961; Gay, 1999; Vermeesch, 2011; El-  
73 belrhiti et al., 2008; Hugenholz & Barchyn, 2012). However, the time series are frequently  
74 incomplete, and, therefore, numerical and experimental investigations have been conducted  
75 in parallel with field experiments. Another drawback is that previous experimental and  
76 numerical studies made use of monodisperse particles (unimodal distribution), whereas  
77 dunes in nature consist of polydisperse grains (heterogenous grain sizes). One way to over-  
78 come those drawbacks is by carrying out experiments with polydisperse grains under wa-  
79 ter, the subaqueous barchans being much faster and smaller than the aeolian dunes (the  
80 former having characteristic lengths and turnover times of centimeters and minutes, e.g.,  
81 Hersen et al., 2002; Franklin & Charru, 2009, 2011; Alvarez & Franklin, 2017).

82 The numerical studies made use of continuum (Schwämmle & Herrmann, 2003; Durán  
83 et al., 2005; Zhou et al., 2019) and discrete (Katsuki et al., 2011) models to compute the  
84 evolution of a bed surface into a dune field, most of them incorporating rules for barchan-  
85 barchan interactions (Lima et al., 2002; E. Parteli & Herrmann, 2003; Katsuki et al., 2005;  
86 Durán et al., 2009). In addition to these techniques, Durán et al. (2009) and Génois, du  
87 Pont, et al. (2013) proposed an agent-based model that makes use of sand- flux balances  
88 and elementary rules for barchan collisions, and Bo and Zheng (2013) used a scale-coupled  
89 model (Zheng et al., 2009) to obtain the probability of occurrence of different types of  
90 barchan-barchan collisions. Those numerical investigations showed that barchan-barchan  
91 collisions lead to corridors of size-selected barchans, pointing toward homogeneous dune  
92 fields. However, model simplifications prevented them from reproducing correctly all barchan-  
93 barchan interactions, and, in addition, there is a lack of numerical studies at the grain  
94 scale (which could give important information for understanding binary interactions, such  
95 as mass transfers between dunes, diffusion of grains within one barchan, and motion of  
96 grains over the barchan surface).

97 The experiments were carried out almost exclusively in water tanks and channels.  
98 Some studies measured the flow disturbances caused by an upstream barchan upon a down-  
99 stream one, such as was done by Bristow et al. (Bristow et al., 2018, 2019, 2020), who  
100 found, among other findings, that turbulence levels increase on the stoss surface of the  
101 downstream dune, enhancing erosion over the downstream dune. Other investigations  
102 measured the evolution of two interacting bedforms, identifying different interaction pat-  
103 terns (Endo et al., 2004; Hersen & Douady, 2005; Bacik et al., 2020; Assis & Franklin,  
104 2020) and mass exchanges at the grain scale (Assis & Franklin, 2021). Endo et al. (2004)  
105 investigated collisions of aligned barchans by varying their mass ratio while maintain-  
106 ing fixed the water flow rate, initial conditions and grain types, and they found three col-  
107 lision patterns which were called merging, exchange and fragmentation-chasing by Assis  
108 and Franklin (2020) (and explained next). Hersen and Douady (2005) investigated the  
109 collisions of off-centered barchans by varying their transverse distances while keeping the  
110 other parameters fixed, and showed that collisions produce smaller barchans, regulat-  
111 ing thus their size when in a barchan field. The experiments of Bacik et al. (2020) were  
112 devoted to the interaction over long times between a pair of two-dimensional dunes in  
113 a circular channel, and they found that turbulent structures of the disturbed flow pre-  
114 vent dune collisions by inducing dune-dune repulsion. Recently, Assis and Franklin (2020,  
115 2021) inquired further into the binary interactions of subaqueous barchans by conduct-  
116 ing experiments in both aligned and off-centered configurations where the water flow rates,  
117 grain types (diameter, density and roundness), pile masses, longitudinal and transverse  
118 distances, and initial conditions were varied, and measurements were made at the bed-  
119 form and grain scales. They found five interaction patterns for both aligned and off-centered  
120 configurations, proposed classification maps, measured the trajectories of individual grains  
121 during barchan-barchan interactions, and found the typical lengths and velocities of grains,  
122 the mass exchanged between barchans, and a diffusive length for some collisions.

123 From the previous works, the most comprehensive classification of barchan-barchan  
124 interactions is the one presented in Assis and Franklin (2020), which identifies: (i) chas-  
125 ing, when collision does not occur, the upstream barchan not reaching the downstream  
126 one; (ii) merging, when collision occurs and the dunes merge; (iii) exchange, when, once  
127 collision takes place, a small barchan is ejected; (iv) fragmentation-chasing, when the down-  
128 stream dune splits without collision taking place and the downstream bedforms outrun  
129 the upstream one; and (v) fragmentation-exchange, when fragmentation initiates, col-  
130 lision takes place, and a small barchan is ejected. The question that persists is if the same  
131 patterns and classification maps proposed by Assis and Franklin (2020) remain valid for  
132 aeolian and Martian barchans (and also other planetary environments), and polydisperse  
133 dunes. While proving the validity for aeolian and Martian barchans is hindered by their  
134 large timescales, that for polydisperse barchans, on the other hand, can be investigated  
135 in the subaqueous case.

136 Concerning dunes of polydisperse grains, Alvarez et al. (2021) investigated exper-  
137 imentally the growth of subaqueous single barchans consisting of bidisperse grains (bi-  
138 modal distribution). In their experiments, single granular piles consisting of bidisperse  
139 mixtures in terms of grain sizes and/or densities were developed into barchan dunes, and  
140 they found that, depending on the mixed grains, either (i) denser, (ii) smaller, or (iii)  
141 smaller and less dense grains tend to accumulate over the barchan surface. They also  
142 found that a transient stripe transverse to the flow direction appears just upstream the  
143 crest of the initial bedform and migrates toward its leading edge until disappearing, that  
144 that line separates a downstream region where segregation is complete from the upstream  
145 region where segregation is still occurring, and that the final barchan morphology is roughly  
146 the same as that of monodisperse barchans. Finally, they proposed that segregation pat-  
147 terns result from a competition between fluid entrainment and ease of rolling, and showed  
148 that grains segregate with a diffusion-like mechanism.

149 Although previous studies explained certain aspects of barchan-barchan interac-  
150 tions, such as the existing patterns, their classification in parameter spaces, and sand re-  
151 distribution during interactions, many others remain to be understood. Among the major  
152 questions still to be investigated, there are the interactions between barchans in the  
153 presence of polydisperse (heterogeneous) grains and the identification of timescales for  
154 barchan-barchan interactions. While the first better represents dunes in the field, the  
155 latter imply a measurement unit for durations of dune-dune interactions.

156 In this paper, we investigate the binary interactions of barchans when grains of two  
157 different sizes are involved, which is a simplified case of real dunes consisting of polydis-  
158 perse grains. For that, we inquired into two specific cases: (i) each bedform consisting  
159 of bidisperse mixtures (bimodal distributions of grains); (ii) each bedform consisting of  
160 a given, but different between them, grain type (two-species monodisperse barchans).  
161 The experiments were conducted in a water channel where grains were poured inside,  
162 forming two conical piles that were afterward deformed by the water flow into barchans  
163 that interacted with each other. The evolution and interactions of bedforms were recorded  
164 by a conventional camera and their morphology was obtained from image processing. We  
165 observe that a transient stripe appears over the dunes in cases of bidisperse mixtures,  
166 just as happens for single bidisperse barchans (Alvarez et al., 2021). We show, for the  
167 first time, that interaction patterns vary with grain concentrations, and that different  
168 interactions exist when each barchan consists of different monodisperse grains (two-species  
169 monodisperse barchans), including collisions in which the upstream barchan is larger than  
170 the downstream one. Finally, we propose a timescale for the interactions of barchans valid  
171 not only for the two-species cases (cases i and ii), but also when only one species is in-  
172 volved (one-species monodisperse barchans). Our results represent a new step toward  
173 understanding complex barchanoid structures found on Earth, Mars and other celestial  
174 bodies.

175 In the following, Section 2 describes the experimental setup and procedure, Sec-  
 176 tion 3 presents the obtained results, and Section 4 presents the conclusions.

## 177 2 Experimental Setup

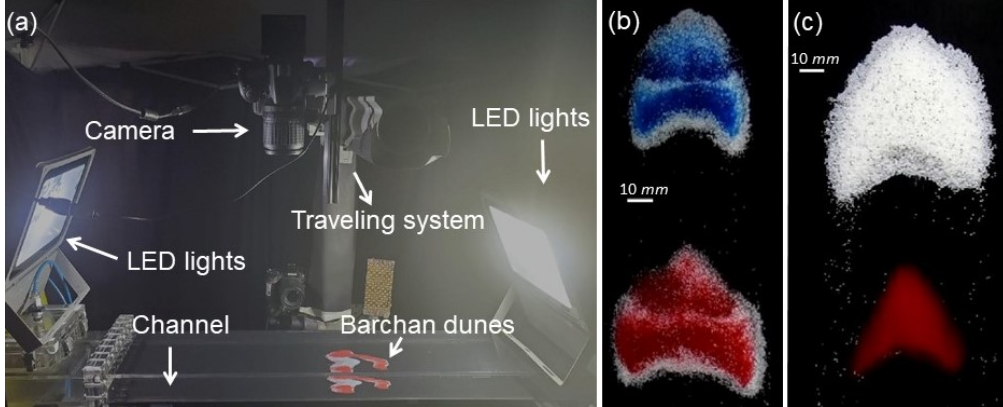


**Figure 1.** (a) Photograph of test section showing the dunes, camera and LED lights; (b) top-view image of two interacting bidisperse barchans (case *e* of Table 1); (c) top-view image of two interacting monodisperse barchans of different granulometry (case *o* of Table 1, of a larger barchan reaching a smaller one); In figures (b) and (c) the flow is from top to bottom.

178 The experimental device consisted basically of a water tank, centrifugal pumps, a  
 179 flow straightener, a 5-m-long closed-conduit channel, a settling tank, and a return line,  
 180 so that we imposed a pressure-driven water flow in closed loop. The channel had a rect-  
 181 angular cross section 160 mm wide by  $2\delta = 50$  mm high, was made of transparent ma-  
 182 terial, and consisted of a 3-m-long entrance section (corresponding to 40 hydraulic di-  
 183 ameters), a 1-m-long test section, and a 1-m-long section connecting the test section  
 184 to the channel exit. With the channel filled with water in still conditions, controlled grains  
 185 were poured inside in order to form two aligned piles consisting of (i) bidisperse mixtures  
 186 (bimodal distributions); (ii) different monodisperse (unimodal) grains (two-species, each  
 187 pile consisting of one single species). In the case of bidisperse mixtures, the grains were  
 188 weighted in the desired proportions and mixed before being poured. Afterward, a spec-  
 189 ified water flow was imposed, deforming each pile into a barchan dune that interacted  
 190 with each other while a camera recorded top view images of the bedforms. No influx of  
 191 grains coming from regions upstream the test section was imposed and, therefore, the  
 192 entire system decreased in mass along time. Using the same terminology of previous works  
 193 (Assis & Franklin, 2020, 2021), we call *impact barchan* the one that was initially upstream  
 194 and *target barchan* the one that was initially downstream. Figure 1a shows a photograph  
 195 of the test section, and Figures 1b and 1c top-view images of two interacting barchans  
 196 consisting each of bidisperse and monodisperse grains, respectively. The layout of the  
 197 experimental device is shown in the supporting information.

198 In our tests, we used tap water at temperatures within 22 and 28 °C and round  
 199 glass beads ( $\rho_s = 2500$  kg/m<sup>3</sup>) with diameters  $0.15 \text{ mm} \leq d_{s1} \leq 0.25 \text{ mm}$  and  $0.40 \text{ mm}$   
 200  $\leq d_{s2} \leq 0.60 \text{ mm}$ , which we call species 1 and 2, respectively. We consider in our com-  
 201 putations the mean values  $d_1 = 0.2 \text{ mm}$  and  $d_2 = 0.5 \text{ mm}$  of  $d_{s1}$  and  $d_{s2}$ , respectively,  
 202 and we used grains of different colors (white, red and blue) in order to track the differ-  
 203 ent species along images (all grains have the same density, see the supporting informa-  
 204 tion for microscopy images of the used grains). We varied the concentration of each grain

205 type ( $\phi_1$  and  $\phi_2$ ) between 0 and 1, the mass ratio of the piles (initial mass of the impact  
 206 barchan  $m_i$  divided by that of the target one  $m_t$ ) between 0.02 and 4, and the water ve-  
 207 locities within  $0.278 \text{ m/s} \leq U \leq 0.347 \text{ m/s}$ , where  $U$  is the cross-sectional mean veloc-  
 208 ity of water. These values correspond to Reynolds numbers based on the channel height,  
 209  $Re = \rho U 2\delta / \mu$ , within  $1.39 \times 10^4$  and  $1.74 \times 10^4$ , where  $\mu$  is the dynamic viscosity and  
 210  $\rho$  the density of the fluid. We computed shear velocities of the undisturbed water flow  
 211 over the channel walls  $u_*$  from measurements with a two-dimensional two-component  
 212 particle image velocimetry (2D2C-PIV) device, and we use  $u_*$  as a reference value for  
 213 fluid shearing even when bedforms are present in the channel. Our measurements show  
 214 values within 0.0159 and 0.0193 m/s and that  $u_*$  follows the Blasius correlation (Schlichting,  
 215 2000). With those values, the Shields number  $\theta = (\rho u_*^2) / ((\rho_s - \rho)gd)$  varied within 0.034  
 216 and 0.127 (where  $g$  is the acceleration of gravity), and the particle Reynolds number  $Re_*$   
 217  $= \rho u_* d / \mu$  within 3 and 10. Because we are interested in the short-range interaction of  
 218 barchans, the initial separation  $\Delta x_d$  was kept close to the diameter of the impact bed-  
 219 form  $D_i$ , with some deviations due to the preparation of initial piles (Assis and Franklin  
 220 (2020) varied considerably  $\Delta x_d$  and observed that the patterns remained the same, the  
 221 only effect being the increase in the duration of the interactions). Table 1 summarizes  
 222 the tested conditions, and complete tables with all the parameters (in dimensional form)  
 223 are available on an open repository (Assis et al., 2021).

224 A digital camera with a lens of 18-140 mm focal distance and F2.8 maximum aper-  
 225 ture was mounted on a traveling system in order to have a top view of the bedforms, and  
 226 lamps of light-emitting diode (LED) were used as light source. The camera was of com-  
 227plementary metal-oxide-semiconductor (CMOS) type with a maximum resolution of 1920  
 228 px  $\times$  1080 px at 60 Hz, and the region of interest (ROI) was set between 1311 px  $\times$  451  
 229 px and 1920 px  $\times$  771 px, for fields of view varying within 354 mm  $\times$  122 mm and 507  
 230 mm  $\times$  122 mm. The acquired images were afterward processed by numerical scripts that  
 231 identified and tracked bedforms and patterns, and were based on Crocker and Grier (1996).  
 232 Movies showing collisions of bidisperse barchans are available in the supporting infor-  
 233 mation and on an open repository (Assis et al., 2021).

### 234 3 Results and discussion

#### 235 3.1 Bidisperse piles

236 We followed the barchans consisting of bidisperse mixtures, for different concen-  
 237 trations of species 1 and 2, and we found patterns similar to those found by Assis and  
 238 Franklin (2020) for monodisperse (one-species) barchans. The obtained patterns are shown  
 239 in Figure 2 for fixed concentrations  $\phi_1 = 0.5$  and  $\phi_2 = 0.5$  in both initial piles (cases *a*  
 240 to *e* in Table 1), and in Figure 3 for concentrations  $\phi_1$  and  $\phi_2$  alternating between ei-  
 241 ther 0.2 or 0.8 (cases *f* to *k* in Table 1). Movies for all cases are available on an open  
 242 repository (Assis et al., 2021), and for cases *b* and *o* in the supporting information.

243 For  $\phi_1 = \phi_2 = 0.5$ , the same interaction patterns of one-species barchans occur (Assis  
 244 & Franklin, 2020), namely the chasing, merging, exchange, fragmentation-chasing and  
 245 fragmentation-exchange patterns (Figures 2e, 2a, 2b, 2d and 2c, respectively). By alter-  
 246 nating  $\phi_1$  and  $\phi_2$  between either 0.2 or 0.8, using the same (Figures 3a, 3b, 3e and 3f,  
 247 corresponding to cases *f*, *g*, *j* and *k* of Table 1) or inverted (Figures 3c and 3d, corre-  
 248 sponding to cases *h* and *i* of Table 1) concentrations for the impact and target barchans,  
 249 and for three values of  $m_i/m_t$  while all the other parameters were kept constant, we ob-  
 250 tained the merging, exchange and fragmentation-exchange patterns. We note that it is  
 251 probable that the chasing and fragmentation-chasing patterns exist also for the concen-  
 252 trations employed. We did not, however, vary the mass ratio in order to investigate this  
 253 specifically.

Case	$\phi_{1t}$	$\phi_{2t}$	$\phi_{1i}$	$\phi_{2i}$	$D_t$	$D_i$	$\Delta x_d$	$Re$	$u_*$	$m_i/m_t$	$t_s$	$t_c$	$Pat$
...	...	...	...	...	mm	mm	mm	...	mm/s	...	s	...	...
a	0.5	0.5	0.5	0.5	63	18	18	$1.56 \times 10^4$	0.0176	0.02	230	0.1	M
b	0.5	0.5	0.5	0.5	61	24	23	$1.56 \times 10^4$	0.0176	0.05	450	0.2	E
c	0.5	0.5	0.5	0.5	56	27	20	$1.56 \times 10^4$	0.0176	0.11	499	0.6	FE
d	0.5	0.5	0.5	0.5	43	30	30	$1.56 \times 10^4$	0.0176	0.43	1537	$\infty$	FC
e	0.5	0.5	0.5	0.5	52	48	39	$1.56 \times 10^4$	0.0176	0.67	10637	$\infty$	C
f	0.8	0.2	0.8	0.2	56	22	21	$1.56 \times 10^4$	0.0176	0.05	482	0.1	E
g	0.2	0.8	0.2	0.8	60	25	21	$1.56 \times 10^4$	0.0176	0.05	318	0.2	M
h	0.8	0.2	0.2	0.8	54	21	21	$1.56 \times 10^4$	0.0176	0.05	215	0.2	E
i	0.2	0.8	0.8	0.2	55	21	23	$1.56 \times 10^4$	0.0176	0.05	893	0.3	$\sim$ FE
j	0.8	0.2	0.8	0.2	53	26	28	$1.56 \times 10^4$	0.0176	0.11	889	0.3	FE
k	0.2	0.8	0.2	0.8	59	30	34	$1.56 \times 10^4$	0.0176	0.25	800	0.2	FE
l	1.0	0.0	0.0	1.0	44	49	39	$1.56 \times 10^4$	0.0176	1.00	989	0.1	U
m	1.0	0.0	0.0	1.0	51	55	29	$1.39 \times 10^4$	0.0159	1.00	870	0.5	U
n	1.0	0.0	0.0	1.0	57	43	34	$1.56 \times 10^4$	0.0176	0.25	596	0.04	U
o	1.0	0.0	0.0	1.0	39	62	34	$1.74 \times 10^4$	0.0193	4.00	1471	0.04	U

**Table 1.** Label of tested cases, initial concentration (mass basis) of each species within the target ( $\phi_{1t}$  and  $\phi_{2t}$ ) and impact ( $\phi_{1i}$  and  $\phi_{2i}$ ) piles, initial diameters of target and impact piles,  $D_t$  and  $D_i$ , respectively, initial separation  $\Delta x_d$ , channel Reynolds number  $Re$ , undisturbed shear velocity  $u_*$ , ratio between initial masses  $m_i/m_t$ , proposed timescale  $t_s$  (Eq. 4 in Subsection 3.3), characteristic time  $t_c$  (shown in Subsection 3.3), and interaction pattern  $Pat$ . C, M, E, FC, FE and U stand for chasing, merging, exchange, fragmentation-chasing, fragmentation-exchange and undefined patterns, respectively.

254 Although the bidisperse piles (mixtures) produce the same interaction patterns ob-  
255 served for one-species barchans, they present some peculiarities in terms of morphody-  
256 namics. Two of those peculiarities are related with grain segregation, as shown by Alvarez  
257 et al. (2021) for single barchans: the accumulation of the smaller grains over the surface  
258 of bedforms, and the appearance of a transient stripe (the narrow band consisting of large  
259 grains), transverse to the flow direction, that initiates upstream the crest of the initial  
260 bedform and migrates toward its leading edge until disappearing. Alvarez et al. (2021)  
261 showed that the transient stripe separates the region where segregation is complete from  
262 that where segregation is ongoing, and the same feature applies here since bidisperse con-  
263 ical piles are being deformed into bidisperse barchans. Another difference is the forma-  
264 tion of a large void (absence of grains) when the impact barchan reaches the target one  
265 in the exchange pattern (Figures 2b and 3a, corresponding to cases *b* and *f* in Table 1).  
266 This void region occurs in the recirculation bubble of the impact barchan and persists  
267 until a baby barchan containing only grains from the target one is ejected. The baby barchan  
268 has roughly the same projected area of the impact barchan when  $\phi_1 = \phi_2 = 0.5$ , but not  
269 necessarily when  $\phi_1 \neq \phi_2$ , and, just after the baby barchan is ejected (at 157 s in Fig-  
270 ure 2b and 155 s in Figure 3a), the parent bedform has an unusual shape, resembling  
271 two elongated barchans containing grains from the target barchan and linked by grains  
272 from the impact one. After some time, the parent bedform attains a barchan shape.

273 Figure 4a presents the time evolution of areas occupied by the void region  $A_{vd}$ , nor-  
274 malized by the total area (projected area)  $A_t$  occupied by grains, for the exchange cases  
275 when  $\phi_1 = \phi_2 = 0.5$  (Figure 2b, case *b*) and  $\phi_1 \neq \phi_2$  (Figure 3a, case *f*). The compu-  
276 tation of areas began when the impact barchan reached the target one, forming a closed  
277 void, and finished when the void was no longer closed, the baby barchan being ejected

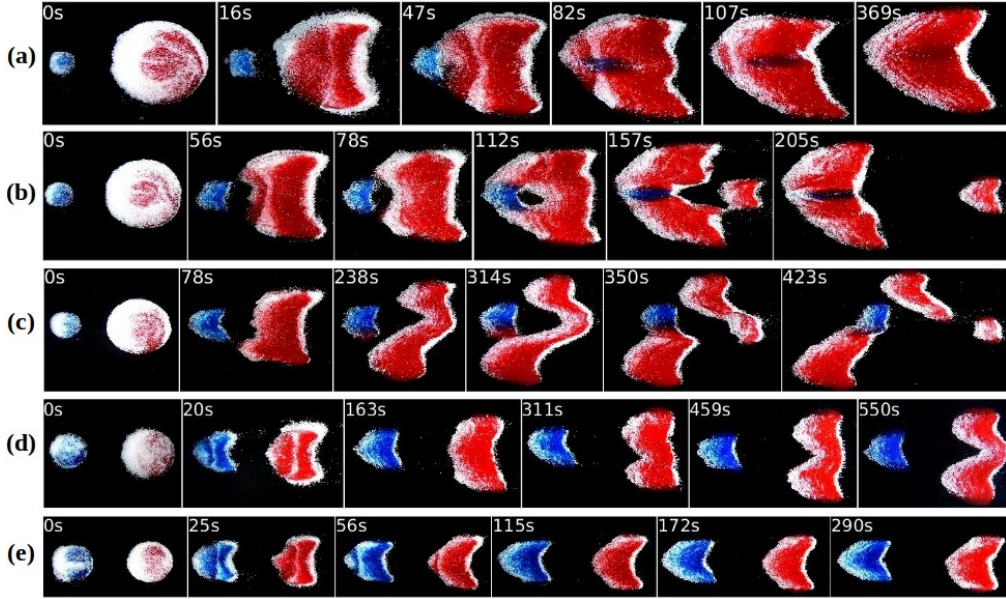


**Figure 2.** Snapshots of interactions of bidisperse barchans for fixed initial concentrations  $\phi_1 = 0.5$  and  $\phi_2 = 0.5$ . In the snapshots, the white (clearer) beads correspond to  $d_2 = 0.5$  mm and red and blue (darker) beads to  $d_1 = 0.2$  mm, the water flow is from left to right, and the corresponding times are shown in each frame. Figures (a) to (e) correspond to cases *a* to *e* of Table 1: (a) merging; (b) exchange; (c) fragmentation-exchange; (d) fragmentation-chasing; (e) chasing.

278 just afterward (see the supporting information for examples of void region detection and  
 279 the time evolution of  $A_{vd}$  in dimensional form). We observe that the void area corresponds  
 280 to 5 to 10% of the projected area occupied by the grains, the void remaining roughly con-  
 281 stant for a certain time and then increasing considerably by the time the baby barchan  
 282 is to be ejected. We observe also that the void is greater when in the presence of a large  
 283 concentration of smaller grains. The reasons and mechanisms by which the void is formed  
 284 remain to be investigated further, but they seem associated with granulometric distri-  
 285 butions, since we had not observed voids in our experiments with one-species barchans  
 286 (Assis & Franklin, 2020, 2021).

287 As a consequence of the aforementioned differences, the resulting patterns in the  
 288 bidisperse case do not necessarily occur under the same conditions as for monodisperse  
 289 barchans. Figure 4b plots the experimental points measured with bidisperse barchans  
 290 in the map proposed by Assis and Franklin (2020) for the aligned case (figure modified  
 291 from Assis & Franklin, 2020), which is drawn in the parameter space consisting of the  
 292 Shields number  $\theta$  and dimensionless particle number  $\xi_N = \Delta_N/\Sigma_N$ , where  $\Delta_N$  is the dif-  
 293 ference and  $\Sigma_N$  the sum of the number of grains forming each pile. For the bidisperse  
 294 case (symbols in Figure 4b),  $\theta$  of each pile was computed for each species (i.e.,  $\theta_1$  and  
 295  $\theta_2$  using  $d_1$  and  $d_2$ , respectively) and then averaged by the number of grains of each species:  
 296  $\theta = N_1\theta_1/N + N_2\theta_2/N$ , where  $N_1$ ,  $N_2$  and  $N$  are the number of grains of species 1, 2,  
 297 and their sum, respectively. In addition, for cases where impact and target barchans had  
 298 different compositions (cases *h* and *i*),  $\theta$  was afterward computed as an averaged weighted  
 299 by the size (total number of grains) of each barchan. We observe that most of points fall  
 300 within the corresponding patterns found in the monodisperse case, or very near the bound-  
 301 aries, but some of them deviate, crossing regions in the map. In general, while the ex-  
 302 change, fragmentation-chasing and fragmentation-exchange tend to remain within their

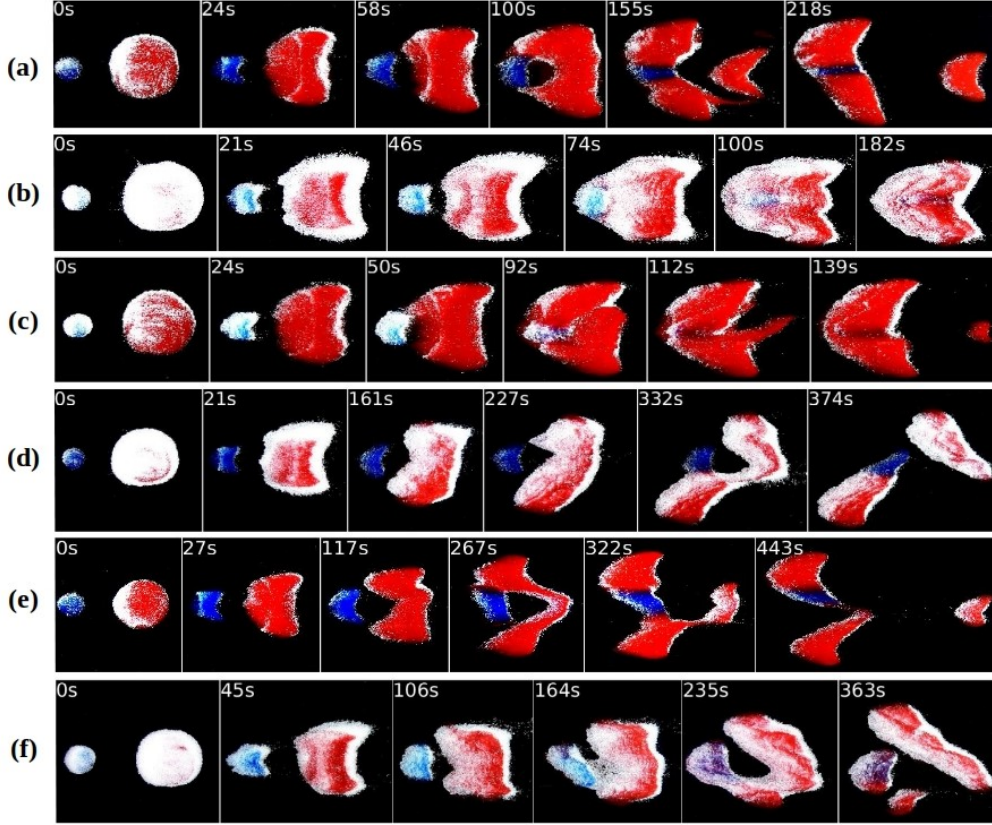


**Figure 3.** Snapshots of interactions of bidisperse barchans for fixed initial concentrations  $\phi_1$  and  $\phi_2$  alternating between either 0.2 or 0.8. In the snapshots, the white (clearer) beads correspond to  $d_2 = 0.5$  mm and red and blue (darker) beads to  $d_1 = 0.2$  mm, the water flow is from left to right, and the corresponding times are shown in each frame. Figures (a) to (f) correspond to cases  $f$  to  $k$  of Table 1: (a) exchange; (b) merging; (c) exchange; (d) fragmentation-exchange; (e) fragmentation-exchange; (f) fragmentation-exchange.

303 respective boundaries, the chasing and merging patterns deviate considerably, the former  
 304 crossing the line and occupying part of the fragmentation-chasing region and the  
 305 latter occupying part of the exchange region. We note that if we had used  $m_i/m_t$  or a  
 306 length ratio (as other authors did, e.g., Endo et al., 2004; Katsuki et al., 2005, 2011; Génois,  
 307 Hersen, et al., 2013) instead of  $\xi_N$ , many of the symbols would be superposed in Figure  
 308 4b even if measured patterns are different, since the mass ratio does not take into con-  
 309 sideration details about granular compositions (see the supporting information for a map  
 310 using  $m_i/m_t$ ). This corroborates, in a certain way, the use of a dimensionless parame-  
 311 ter based on the number of elements ( $\xi_N$ ) rather than  $m_i/m_t$ .

312 In particular, we analyzed the projected areas occupied by grains during some ex-  
 313 change patterns. For monodisperse dunes, Assis and Franklin (2020, 2021) showed that  
 314 the impact barchan first merges with the target one, and afterward a new barchan (baby  
 315 barchan) is ejected (the remaining bedform being the parent barchan). In addition, Assis  
 316 and Franklin (2020) showed that the baby barchan has roughly the same size of the im-  
 317 pact barchan, but contains grains only from the target one. In the case of bidisperse mix-  
 318 tures, a similar behavior happens. Figure 5 shows the projected areas of bedforms dur-  
 319 ing the exchange processes of Figures 2b, 3a and 3c (cases  $a$ ,  $f$  and  $h$ , corresponding to

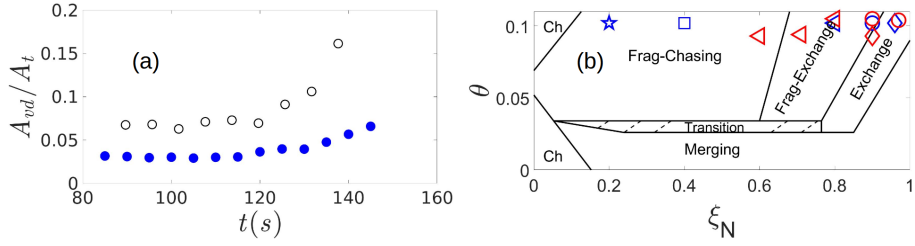


**Figure 4.** (a) Area occupied by the void region  $A_{vd}$  normalized by the total area (projected)  $A_t$  occupied by grains as a function of time. Solid blue circles correspond to the exchange pattern when  $\phi_1 = \phi_2 = 0.5$  (Figure 2b, case *b*) and open black symbols when  $\phi_1 \neq \phi_2$  (Figure 3a, case *f*). (b) Interaction patterns for barchans of bidisperse mixtures: classification map proposed by Assis and Franklin (2020) for monodisperse barchans, over which we superposed the experimentally obtained chasing - Ch ( $\star$ ), merging ( $\diamond$ ), exchange ( $\circ$ ), fragmentation-chasing ( $\square$ ), and fragmentation-exchange ( $\triangleleft$ ) patterns for the bidisperse case. Blue color corresponds to  $\phi_1 = \phi_2 = 0.5$  (Figure 2) and red to  $\phi_1 \neq \phi_2$  (Figure 3). Figure modified from Assis and Franklin (2020).

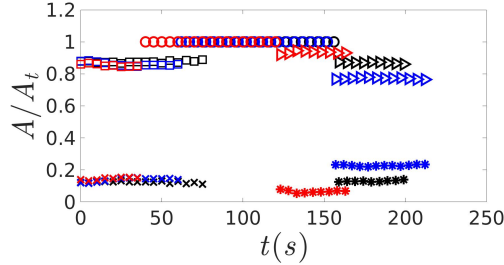


**Figure 5.** Projected areas, normalized by  $A_t$ , of impact (x), target ( $\square$ ), merged ( $\circ$ ), parent ( $\triangleright$ ), and baby ( $\ast$ ) barchans, respectively, as functions of time, during exchange processes. Black, blue and red colors correspond to cases *a*, *f* and *h* (Figures 2b, 3a and 3c), respectively.

320 black, blue and red colors, respectively. A graphic in dimensional form is available in the  
 321 supporting information). While the baby barchan does not contain grains from the impact  
 322 barchan (seen directly from Figures 2b, 3a and 3c), Figure 5 shows that their areas  
 323 are roughly the same (for the analyzed cases).

324 In summary, we show that in the mixed case the interaction patterns and their dyn-  
 325 amics are roughly the same as in the monodisperse case; however, although the maps  
 326 proposed in Assis and Franklin (2020) bring valuable information for classifying the barchan-  
 327 barchan interactions, results with polydisperse dunes can deviate from the proposed bound-  
 328 aries. Therefore, the distribution of grains within the barchans should be taken into con-  
 329 sideration in analyses of barchan-barchan interactions occurring in nature.

### 330 3.2 Two-species monodisperse piles

331 We followed the initially monodisperse bedforms consisting each of different grains,  
 332 and we found different patterns. These patterns, cases *l* to *o* in Table 1, are shown in  
 333 Figure 6, which presents snapshots of barchans at some instants during their interactions,  
 334 including a collision where the impact barchan was larger than the target one (see the  
 335 supporting information or Assis et al. (2021) for movies of collisions). For this specific

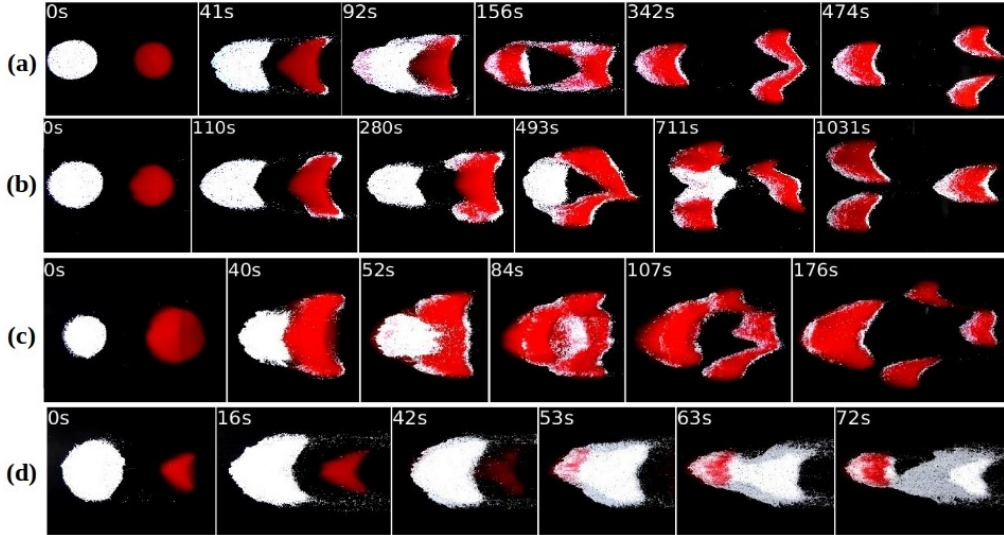


**Figure 6.** Snapshots of barchan interactions for initially monodisperse piles of different grains (two-species monodisperse piles). In the snapshots, the upstream pile consists of white (clearer) beads with  $d_2 = 0.5$  mm and the downstream pile of red (darker) beads with  $d_1 = 0.2$  mm, the water flow is from left to right, and the corresponding times are shown in each frame. Figures (a) to (d) correspond to cases *l* to *o* of Table 1.

336 case, we made use of larger grains in the impact dune since the celerity of barchans varies  
 337 with the diameter of their grains (Franklin & Charru, 2011, see also Eq. 2 in Subsection  
 338 3.3).

339 For all the interactions shown in Figure 6, the impact barchan consisted of grains  
 340 of species 2 ( $d_2 = 0.5$  mm) in white color and the target barchan of species 1 ( $d_1 = 0.2$   
 341 mm) in red color. In Figure 6a (case *l* in Table 1), the barchans collide, forming a large  
 342 void in the recirculation region when they touch each other, and with the larger grains  
 343 moving over the smaller ones that, in their turn, emerge at the toe of the resulting bed-  
 344 form (at 92 s). Afterward (at 156 s), the smaller grains having accumulated over the sur-  
 345 face of the resulting bedform, the latter begins to split in what seems, initially, two barchans  
 346 linked by two large branches. Finally (at 474s), they split in three barchans (one upstream  
 347 and two downstream, in a staggered configuration) consisting each of bidisperse grains.  
 348 Figures 7a and 7b show the time evolution of projected areas of dunes for cases *l* and  
 349 *m*, respectively (Figures 7c and 7d in dimensionless form, normalized by  $A_t$ ). Interest-  
 350 ingly, we can observe from Figure 7a that, after the dunes collide (at  $\sim 90$  s), the pro-  
 351 jected area of the resulting bedform first increases and then decreases. This is due, re-  
 352 spectively, to larger grains migrating over the smaller ones and spreading over the dune,  
 353 and afterward the smaller grains accumulating over the dune surface and decreasing the  
 354 projected area. In addition, Figure 7a shows that the two final downstream barchans have  
 355 roughly the same size.

356 In Figure 6b (case *m* in Table 1), the behavior is similar to that of Figure 6a, the  
 357 main difference being that the final state is inverted: two upstream barchans and one  
 358 downstream barchan, in a staggered configuration. In both cases *l* and *m* the initial masses  
 359 are the same (the initial diameter of the impact pile being larger since it consists of larger  
 360 grains), only the fluid velocity is different, being higher for case *l*. Why the behavior changes  
 361 by changing the water velocity remains to be investigated (we do not advance an expla-  
 362 nation for the moment). However, we can observe from Figure 7b the same increase and

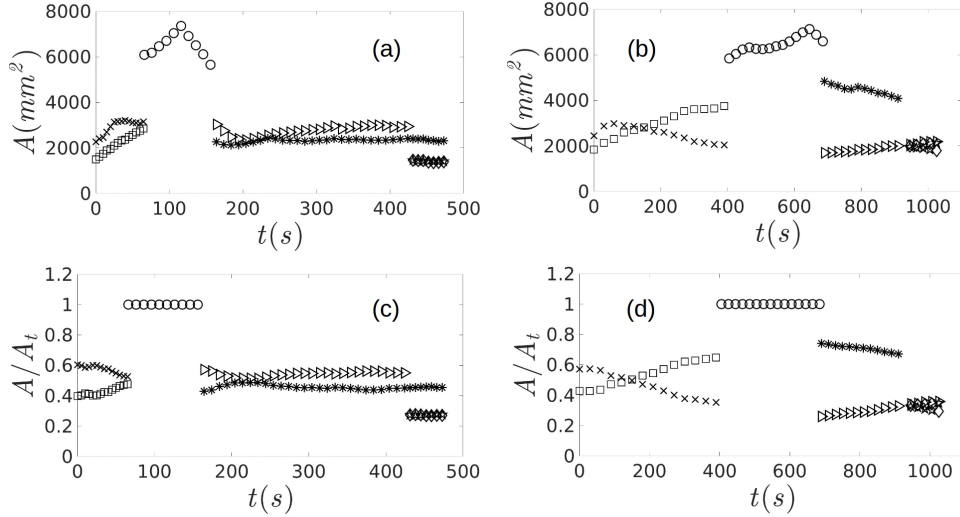


**Figure 7.** Projected areas of impact (x), target ( $\square$ ), merged ( $\circ$ ), upstream after splitting ( $*$ ), parent ( $\triangleright$ ), and baby barchans ( $\diamond$  and  $\star$ ), respectively, during undefined-exchange processes for (a) and (c) case  $l$  (Figure 6a) and (b) and (d) case  $m$  (Figure 6b). Figures (a) and (b) are in dimensional and (c) and (d) in dimensionless form (normalized by  $A_t$ ).

363 decrease of the projected area after the dunes have collided (at  $\sim 400$  s), that the result-  
 364 tant bedform splits first in one larger upstream and one smaller downstream bedform  
 365 (at  $\sim 700$  s), and that the upstream bedform splits in two dunes later (at  $\sim 950$  s). We  
 366 end finally with three barchans of roughly the same size.

367 Figure 6c corresponds to case  $n$  of Table 1, and shows a collision in which three barchans  
 368 are ejected from the merged bedform. This case resembles the exchange pattern (Assis  
 369 & Franklin, 2020, 2021), with the difference that three baby barchans are ejected, one  
 370 aligned and two in staggered configuration.

371 Finally, Figure 6d corresponds to case  $o$  of Table 1, the unusual case of a collision  
 372 of a larger impact with a smaller target barchan. As far as we know, this is the first time  
 373 that this kind of collision is reported (see the supporting information or Assis et al. (2021)  
 374 for a movie of this interaction), Groh et al. (2009) having measured the collision of a larger  
 375 upstream dune with a smaller downstream one, in the 2D case, by placing initially the  
 376 latter in the recirculation region of the former, thus forcing collision (in addition to hav-  
 377 ing, apparently, entrance effects in their test section). We observe that, as the impact  
 378 barchan gets closer to the target one, the latter becomes more elongated, while grains  
 379 leaving the horns of the impact barchan are entrained further downstream and are not  
 380 incorporated by the target barchan. During the collision ( $t \approx 48$  s), the larger grains move  
 381 over the smaller ones, which, in their turn, emerge at the toe of the resulting bedform.  
 382 Finally, a monodisperse baby barchan consisting of only larger grains is ejected from the  
 383 merged bedform (grains from the impact dune, different from all cases reported previ-  
 384 ously), resulting, in fact, of larger grains being entrained further downstream. The re-  
 385 maining grains form an upstream bidisperse barchan with smaller grains populating its  
 386 upper surface.

387 Figure 8 shows the time evolution of projected areas occupied by white and red grains  
 388 for case  $o$ . From Figure 8a, we observe an initial increase of both areas due to the spread-  
 389 ing of the initial conical pile (being deformed into barchan dunes), with a time interval  
 390 when areas remain roughly constant. When the larger dune approaches the smaller one,

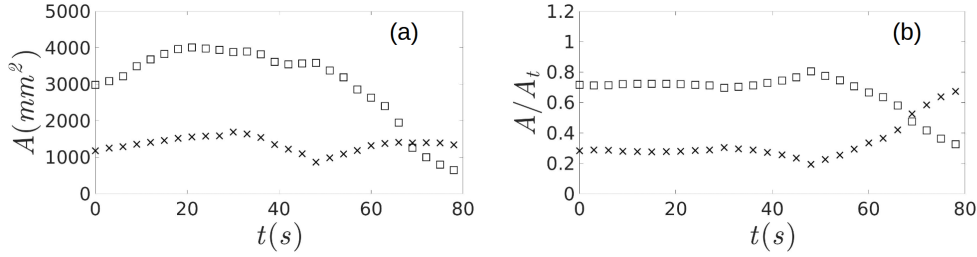


**Figure 8.** Time evolution of projected areas occupied by white (□) and red (x) grains for case  $o$  (Figure 6d), in (a) dimensional form and (b) normalized by  $A_t$ . OBS: the monolayer consisting of white grains observed in Figure 6d was neglected.

391 the vortex on the recirculation region of the former entrains grains from the latter to-  
 392 ward its lee face. Because the larger grains move easier over the smaller ones (Alvarez  
 393 et al., 2021), these remain on the bottom of the impact barchan until they emerge at the  
 394 toe of the impact one, being again exposed to the fluid flow. When the dunes collide,  
 395 the white grains then move over the red (smaller) ones, which appear at the toe of the  
 396 resulting bedform. This “swallowing” process appears in Figure 8 as a decrease followed  
 397 by an increase of the area occupied by red grains within  $30 \text{ s} < t < 70 \text{ s}$ . Finally, by the  
 398 end of the collisional process ( $t \approx 70 \text{ s}$  on), a greater number of larger (white) grains are  
 399 exposed to the fluid flow and are either entrained further downstream or form a mono-  
 400 layer between both barchans, which makes the area occupied by the larger (white) grains  
 401 to decrease considerably (the monolayer being neglected in Figure 8). By considering Fig-  
 402 ure 6d, we observe that a significant amount of larger (white) grains is entrained down-  
 403 stream (white grains leaving the horns, and also the reduction in the area occupied by  
 404 the white grains).

405 In common for cases  $l$  to  $o$ , the larger grains move over the smaller ones, being en-  
 406 trained further downstream and/or accumulating on the lee face and forming a carpet  
 407 for the smaller grains. The same mechanism proposed by Alvarez et al. (2021) seems to  
 408 apply here, i.e., the segregation results from a competition between fluid entrainment  
 409 and ease of rolling. Other than that, we do not advance more explanations for the pat-  
 410 terns shown in Figure 6, but we propose, however, a timescale that applies to all cases  
 411 investigated and is presented in Subsection 3.3.

### 412 3.3 Timescale

413 A question that remained to be answered for barchan-barchan interactions even  
 414 in monodisperse conditions (Endo et al., 2004; Hersen & Douady, 2005; Assis & Franklin,  
 415 2020, 2021), and that can now be investigated for bidisperse barchans, is the existence  
 416 of a proper timescale for the problem. In the following, we propose a timescale and eval-  
 417 uate it in the subaqueous case. A reasonable timescale for the binary interaction of dunes  
 418 can be built as their initial separation  $\Delta x_d$  divided by their relative velocity  $\Delta V_d$ ,

$$t_s = \frac{\Delta x_d}{\Delta V_d} \quad (1)$$

419 where  $\Delta V_d$  is the difference between the celerities  $V_d$  of impact and target barchans (at  
 420 the beginning of the interaction), and  $t_s$  represents a typical time for the collision of barchans  
 421 (faster for closer barchans with stronger relative velocities). Franklin and Charru (2011)

422 investigated the celerities of subaqueous barchans by varying water velocities, grain types,  
 423 and dune sizes, and found that

$$\frac{V_d}{V_{ref}} = 280 Re_s \frac{d}{L} (\theta - \theta_{th})^n \quad (2)$$

424 where  $d$  is the mean grain diameter,  $L$  is the barchan length,  $\theta_{th}$  is the threshold value  
 425 of the Shields number for incipient motion,  $n$  is an exponent,  $Re_s = \rho U_s d / \mu$ , and  $V_{ref}$   
 426  $= ((S-1)gd)^{1/2}$ , with  $S = \rho_s / \rho$  and  $U_s$  the settling velocity of particles. For water flows  
 427 not far from the bedload threshold, Franklin and Charru (2011) found that  $n = 5/2$ , while  
 428 the classical value for similar relations is  $n = 3/2$ , which have proven to work well for  
 429 aeolian dunes (Bagnold, 1941), usually far from the threshold. Therefore, by assuming  
 430 that  $n = 3/2$  far from threshold, Eq. 2 implies that  $V_d \sim d$ . Close to the threshold and  
 431 in turbulent regime,  $(\theta - \theta_{th})^n$  is of lower asymptotic order than  $d^{-n}$ , since  $\theta_{th}$  is an un-  
 432 known function of  $d$ . Therefore,  $V_d \sim d^a$ ,  $a > 0$ . By assuming that  $a \approx 1$  for the sub-  
 433 aqueous case (in order to match the aeolian scaling), both cases give  $V_d \sim d$ . In fact, we  
 434 observe in our experiments that, all else being fixed, dunes composed of larger particles  
 435 move faster, with  $V_d$  varying approximately with  $d$ . We note that Eq. 2 was obtained  
 436 by Franklin and Charru (2011) for  $Re$  of the order of  $10^4$  ( $13900 \leq Re \leq 23100$ ),  $0.12$   
 437  $\text{mm} \leq d \leq 0.51 \text{ mm}$ ,  $1 \leq Re_* \leq 11$ , and  $\rho_p = 2600$  and  $3760 \text{ kg/m}^3$ , which are limited  
 438 conditions, mainly in terms of  $Re$  and  $Re_*$ . Because in the present experiments  $Re_*$  varies  
 439 within 3 and 10 (typical of the subaqueous case), Eq. 2 is clearly valid for our data. How-  
 440 ever, Eq. 2 may be improper for higher values of  $Re_*$ , having a different dependency on  
 441  $Re_s$  and changing the value of the exponent  $a$ , which might even assume negative val-  
 442 ues.

443 Observing that the diameter of the initial pile  $D$  is proportional to  $L$ , and consid-  
 444 ering the mean diameter and density as in Alvarez et al. (2021),  $\bar{d} = (\phi_1/d_1 + \phi_2/d_2)^{-1}$   
 445 and  $\bar{\rho}_s = \phi_1 \rho_1 + \phi_2 \rho_2$ , respectively, we obtain

$$\Delta V_d \sim u_* \left| \frac{\bar{d}_t}{D_t} - \frac{\bar{d}_i}{D_i} \right| \frac{1}{S} \quad (3)$$

446 where  $\bar{d}_i$  and  $\bar{d}_t$  represent the mean diameter of grains forming impact and target barchans,  
 447 respectively, and  $D_i$  and  $D_t$  are the initial diameters of the projected areas of impact  
 448 and target bedforms, respectively. Finally,

$$t_s = \frac{\Delta x_d S}{u_*} \left| \frac{\bar{d}_t}{D_t} - \frac{\bar{d}_i}{D_i} \right|^{-1} \quad (4)$$

449 By normalizing the time interval that barchans take to complete their interaction  
 450  $\Delta t$  by the proposed timescale  $t_s$ , we obtain the characteristic time for interactions  $t_c =$   
 451  $\Delta t / t_s$  (values shown in Table 1). The initial instant for  $\Delta t$  is when the flow starts and  
 452 the final instant when the interaction reaches a stage characteristic of the considered pat-  
 453 tern. In cases with collision (merging, exchange and fragmentation-exchange), the final  
 454 instant is when collision takes place, and in cases without collision (chasing and fragmentation-  
 455 chasing), the final time is much larger than the duration of tests and we consider  $\Delta t$  as  
 456 tending to infinity. In general, we observe the following characteristic times for interac-  
 457 tions:

- 458 •  $0.04 \leq t_c < 2$  for cases with collisions, i.e., the merging, exchange, fragmentation-  
 459 exchange (by considering also the one-species monodisperse barchans presented  
 460 in Assis and Franklin (2020, 2021)) and the undefined patterns of the two-species  
 461 monodisperse barchans;

- $t_c = \infty$  for the chasing and fragmentation-chasing patterns.

Because only cases  $n$  and  $o$  (two-species monodisperse barchans) present  $t_c = 0.04 < 0.1$  and only one fragmentation-exchange pattern for one-species monodisperse barchans (Assis & Franklin, 2021) presents  $t_c = 1.7 > 1$ , we obtained, in general, that  $t_c = O(0.1)$ , where  $O()$  stands for "order of magnitude". This characteristic time holds for the barchans of same monodisperse composition (one species) presented in Assis and Franklin (2020, 2021), for the barchans consisting of bidisperse mixtures, and for the barchans consisting of different monodisperse grains.

The proposed timescale was verified only for subaqueous barchans, which present differences in the fundamental transport mechanism (bedload) when compared to aeolian dunes. Under water, the grains are entrained directly by the fluid and move by rolling and sliding, traveling distances of some grain diameters (between resting times), while in a gaseous environment they effectuate ballistic flights in the main flow direction over distances much larger than the grain diameter. In addition, the timescale is based on Eq. 2, which is valid for the subaqueous case, but not necessarily for other environments. However, the timescale that we propose is based on physical arguments, being basically the initial separation of barchans divided by their relative velocity. Therefore, although we cannot directly evaluate the timescale in other environments for which long-time measurements do not exist, we believe that it remains a reasonable reference. If the proposed timescale proves to be valid for other environments, it will allow the prediction of durations of barchan-barchan interactions and, more generally, provide a scaling for the evolution of dune fields on terrestrial deserts and other planetary environments.

The effect of polydisperse grains on barchan-barchan interactions and the existence of a proper timescale are two questions that were unexplored until now. In this paper, we investigated these issues by using bidisperse grains in a water channel. Other than the observation of a stratification process already reported by Alvarez et al. (2021) in the case of single dunes, we showed, for the first time, that the interaction patterns vary with grain concentrations, and that different interactions exist when each barchan consists of different monodisperse grains. In addition, we found the conditions for a collision in which the upstream barchan is larger than the downstream one, and we propose a timescale for the interactions of both monodisperse and bidisperse barchans. Our results shed light on those two questions, even if our findings remain to be investigated in other environments.

## 4 Conclusions

In this paper, we investigated experimentally the dune-dune interactions for barchans consisting of (i) bidisperse mixtures and (ii) different monodisperse grains (one type for each barchan). The experiments were conducted in a water channel where two barchans interacted with each other while filmed by a camera, and the bedform morphologies and duration of interactions were obtained from image processing. We observed that a transient stripe appears over the dunes in cases of bidisperse mixtures, as also happens for single bidisperse barchans (Alvarez et al., 2021). We showed, for the first time, that interaction patterns vary with grain concentrations, and that different interactions exist when each barchan consists of different monodisperse grains (two-species monodisperse barchans). For the latter, we obtained one very peculiar and unreported case by using larger grains in the impact barchan: the collision of a larger upstream barchan with a smaller downstream one, which showed a different grain distribution in the resulting bedform once the collision had taken place. Finally, we proposed a timescale for the interactions of both monodisperse and bidisperse barchans (cases i and ii, and also one-species monodisperse barchans). The identification of such timescale represents a new step for predicting the duration of binary interactions and, more generally, scaling the evolution of dune fields on Earth, Mars and other planetary environments.

513 **Open Research**

514 Data (digital images) supporting this work were generated by ourselves and are  
 515 available in Mendeley Data (Assis et al., 2021) under the CC-BY-4.0 license. The  
 516 numerical scripts used to process the images are also available in Mendeley Data  
 517 (Assis et al., 2021) under the CC-BY-4.0 license.

518 **Acknowledgments**

519 The authors are grateful to FAPESP (Grant Nos. 2016/18189-0, 2018/14981-7  
 520 and 2019/10239-7) for the financial support provided.

521 **References**

- 522 Alvarez, C. A., Cúñez, F. D., & Franklin, E. M. (2021). Growth of barchan dunes of  
 523 bidispersed granular mixtures. *Phys. Fluids*, *33*(5), 051705.
- 524 Alvarez, C. A., & Franklin, E. M. (2017, Dec). Birth of a subaqueous barchan  
 525 dune. *Phys. Rev. E*, *96*, 062906. Retrieved from [https://link.aps.org/doi/](https://link.aps.org/doi/10.1103/PhysRevE.96.062906)  
 526 [10.1103/PhysRevE.96.062906](https://link.aps.org/doi/10.1103/PhysRevE.96.062906) doi: 10.1103/PhysRevE.96.062906
- 527 Assis, W. R., Cúñez, F. D., & Franklin, E. M. (2021). Experimental data on  
 528 barchan-barchan interaction with bidisperse grains [Dataset][Software]. *Mende-*  
 529 *ley Data*, <http://dx.doi.org/10.17632/sbjtzbzh9k>. doi: 10.17632/sbjtzbzh9k
- 530 Assis, W. R., & Franklin, E. M. (2020). A comprehensive picture for binary interac-  
 531 tions of subaqueous barchans. *Geophys. Res. Lett.*, *47*(18), e2020GL089464.
- 532 Assis, W. R., & Franklin, E. M. (2021). Morphodynamics of barchan-barchan inter-  
 533 actions investigated at the grain scale. *J. Geophys. Res.: Earth Surf.*, *126*(8),  
 534 e2021JF006237.
- 535 Bacik, K. A., Lovett, S., Caulfield, C.-c. P., & Vriend, N. M. (2020, Feb). Wake  
 536 induced long range repulsion of aqueous dunes. *Phys. Rev. Lett.*, *124*, 054501.  
 537 Retrieved from [https://link.aps.org/doi/10.1103/PhysRevLett.124](https://link.aps.org/doi/10.1103/PhysRevLett.124.054501)  
 538 [.054501](https://link.aps.org/doi/10.1103/PhysRevLett.124.054501) doi: 10.1103/PhysRevLett.124.054501
- 539 Bagnold, R. A. (1941). *The physics of blown sand and desert dunes*. London: Chap-  
 540 man and Hall.
- 541 Bo, T. L., & Zheng, X. J. (2013). Collision behaviors of barchans in aeolian dune  
 542 fields. *Environ. Earth. Sci.*, *70*, 2963-2970.
- 543 Bristow, N. R., Blois, G., Best, J. L., & Christensen, K. T. (2018). Turbulent flow  
 544 structure associated with collision between laterally offset, fixed-bed barchan  
 545 dunes. *J. Geophys. Res.-Earth*, *123*(9), 2157-2188.
- 546 Bristow, N. R., Blois, G., Best, J. L., & Christensen, K. T. (2019). Spatial scales  
 547 of turbulent flow structures associated with interacting barchan dunes. *J. Geo-*  
 548 *phys. Res.-Earth*, *124*(5), 1175-1200.
- 549 Bristow, N. R., Blois, G., Best, J. L., & Christensen, K. T. (2020). Secondary flows  
 550 and vortex structure associated with isolated and interacting barchan dunes. *J.*  
 551 *Geophys. Res.-Earth*, *125*(2), e2019JF005257.
- 552 Claudin, P., & Andreotti, B. (2006). A scaling law for aeolian dunes on Mars,  
 553 Venus, Earth, and for subaqueous ripples. *Earth Plan. Sci. Lett.*, *252*, 20-44.
- 554 Crocker, J. C., & Grier, D. G. (1996). Methods of digital video microscopy for col-  
 555 loidal studies. *Journal of Colloid and Interface Science*, *179*(1), 298-310.
- 556 Durán, O., Schwämmle, V., & Herrmann, H. (2005, Aug). Breeding and solitary  
 557 wave behavior of dunes. *Phys. Rev. E*, *72*, 021308. Retrieved from [https://](https://link.aps.org/doi/10.1103/PhysRevE.72.021308)  
 558 [link.aps.org/doi/10.1103/PhysRevE.72.021308](https://link.aps.org/doi/10.1103/PhysRevE.72.021308) doi: 10.1103/PhysRevE  
 559 [.72.021308](https://link.aps.org/doi/10.1103/PhysRevE.72.021308)
- 560 Durán, O., Schwämmle, V., Lind, P. G., & Herrmann, H. (2009). The dune size dis-  
 561 tribution and scaling relations of barchan dune fields. *Granular Matter*, *11*, 7-  
 562 11.

- 563 Elbelrhiti, H., Andreotti, B., & Claudin, P. (2008). Barchan dune corridors: Field  
564 characterization and investigation of control parameters. *Journal of Geophysical*  
565 *Research: Earth Surface*, 113(F2).
- 566 Elbelrhiti, H., Claudin, P., & Andreotti, B. (2005). Field evidence for surface-wave-  
567 induced instability of sand dunes. *Nature*, 437(04058).
- 568 Endo, N., Taniguchi, K., & Katsuki, A. (2004). Observation of the whole process  
569 of interaction between barchans by flume experiments. *Geophys. Res. Lett.*,  
570 31(12).
- 571 Franklin, E. M., & Charru, F. (2009). Morphology and displacement of dunes in a  
572 closed-conduit flow. *Powder Technology*, 190, 247-251.
- 573 Franklin, E. M., & Charru, F. (2011). Subaqueous barchan dunes in turbulent shear  
574 flow. Part 1. Dune motion. *J. Fluid Mech.*, 675, 199-222.
- 575 Gay, S. P. (1999). Observations regarding the movement of barchan sand dunes in  
576 the nazca to tanaca area of southern peru. *Geomorphology*, 27(3), 279 - 293.
- 577 G enois, M., du Pont, S. C., Hersen, P., & Gr egoire, G. (2013). An agent-based  
578 model of dune interactions produces the emergence of patterns in deserts. *Geo-*  
579 *phys. Res. Lett.*, 40(15), 3909-3914.
- 580 G enois, M., Hersen, P., du Pont, S., & Gr egoire, G. (2013). Spatial structuring  
581 and size selection as collective behaviours in an agent-based model for barchan  
582 fields. *Eur. Phys. J. B*, 86(447).
- 583 Groh, C., Rehberg, I., & Kruelle, C. A. (2009). How attractive is a barchan dune?  
584 *New J. Phys.*, 11(2), 023014.
- 585 Herrmann, H. J., & Sauermann, G. (2000). The shape of dunes. *Physica A (Amster-*  
586 *dam)*, 283, 24-30.
- 587 Hersen, P. (2004). On the crescentic shape of barchan dunes. *Eur. Phys. J. B*,  
588 37(4), 507-514.
- 589 Hersen, P., Andersen, K. H., Elbelrhiti, H., Andreotti, B., Claudin, P., & Douady,  
590 S. (2004, Jan). Corridors of barchan dunes: Stability and size selection. *Phys.*  
591 *Rev. E*, 69, 011304. Retrieved from [https://link.aps.org/doi/10.1103/](https://link.aps.org/doi/10.1103/PhysRevE.69.011304)  
592 [PhysRevE.69.011304](https://link.aps.org/doi/10.1103/PhysRevE.69.011304) doi: 10.1103/PhysRevE.69.011304
- 593 Hersen, P., & Douady, S. (2005). Collision of barchan dunes as a mechanism of size  
594 regulation. *Geophys. Res. Lett.*, 32(21).
- 595 Hersen, P., Douady, S., & Andreotti, B. (2002, Dec). Relevant length  
596 scale of barchan dunes. *Phys. Rev. Lett.*, 89, 264301. Retrieved from  
597 <https://link.aps.org/doi/10.1103/PhysRevLett.89.264301> doi:  
598 10.1103/PhysRevLett.89.264301
- 599 Hugenholtz, C. H., & Barchyn, T. E. (2012). Real barchan dune collisions and ejection  
600 s. *Geophys. Res. Lett.*, 39(2).
- 601 Katsuki, A., Kikuchi, M., Nishimori, H., Endo, N., & Taniguchi, K. (2011). Cellular  
602 model for sand dunes with saltation, avalanche and strong erosion: collisional  
603 simulation of barchans. *Earth Surf. Process. Landforms*, 36(3), 372-382.
- 604 Katsuki, A., Nishimori, H., Endo, N., & Taniguchi, K. (2005). Collision dynamics of  
605 two barchan dunes simulated using a simple model. *J. Phys. Soc. Jpn.*, 74(2),  
606 538-541.
- 607 Kocurek, G., Ewing, R. C., & Mohrig, D. (2010). How do bedform patterns arise?  
608 new views on the role of bedform interactions within a set of boundary condi-  
609 tions. *Earth Surf. Process. Landforms*, 35(1), 51-63.
- 610 Lima, A., Sauermann, G., Herrmann, H., & Kroy, K. (2002). Modelling a dune field.  
611 *Physica A*, 310(3), 487-500. Retrieved from [https://www.sciencedirect](https://www.sciencedirect.com/science/article/pii/S0378437102005460)  
612 [.com/science/article/pii/S0378437102005460](https://www.sciencedirect.com/science/article/pii/S0378437102005460)
- 613 Norris, R. M., & Norris, K. S. (1961). Algodones Dunes of Southeastern California.  
614 *GSA Bulletin*, 72(4), 605-619.
- 615 Parteli, E., & Herrmann, H. (2003). A simple model for a transverse dune field.  
616 *Physica A*, 327(3), 554-562.
- 617 Parteli, E. J. R., & Herrmann, H. J. (2007, Oct). Dune formation on the present

- 618 mars. *Phys. Rev. E*, *76*, 041307. Retrieved from [https://link.aps.org/doi/](https://link.aps.org/doi/10.1103/PhysRevE.76.041307)  
619 [10.1103/PhysRevE.76.041307](https://doi.org/10.1103/PhysRevE.76.041307) doi: 10.1103/PhysRevE.76.041307
- 620 Schlichting, H. (2000). *Boundary-layer theory*. New York: Springer.
- 621 Schwämmle, V., & Herrmann, H. J. (2003). Solitary wave behaviour of sand dunes.  
622 *Nature*, *426*, 619-620.
- 623 Vermeesch, P. (2011). Solitary wave behavior in sand dunes observed from space.  
624 *Geophys. Res. Lett.*, *38*(22).
- 625 Zheng, X. J., Bo, T. L., & Zhu, W. (2009). A scale-coupled method for simulation  
626 of the formation and evolution of aeolian dune field. *Int. J. Nonlinear Sci. Numer. Simul.*, *10*(3), 387-396.
- 627
- 628 Zhou, X., Wang, Y., & Yang, B. (2019). Three-dimensional numerical simulations of  
629 barchan dune interactions in unidirectional flow. *Particul. Sci. Technol.*, *37*(7),  
630 835-842.

# Supporting Information for “Revealing the intricate dune-dune interactions of bidisperse barchans”

An edited version of this paper was published by AGU. Copyright (2021) American Geophysical Union. Assis, W. R., Cúñez, F. D. and Franklin, E. M. (2022). Revealing the intricate dune-dune interactions of bidisperse barchans. *Journal of Geophysical Research: Earth Surface*, 127, e2021JF006588. <https://doi.org/10.1029/2021JF006588>

To view the published open abstract, go to <https://doi.org/10.1029/2021JF006588>.

W. R. Assis<sup>1</sup>, F. D. Cúñez<sup>2</sup>, E. M. Franklin<sup>1</sup>

<sup>1</sup>School of Mechanical Engineering, UNICAMP - University of Campinas, Rua Mendeleev, 200, Campinas, SP, Brazil

<sup>2</sup>Department of Earth and Environmental Sciences, University of Rochester, Rochester, NY 14627, USA

## Contents of this file

1. Figures S1 to S8

## Additional Supporting Information (Files uploaded separately)

1. Captions for Movies S1 to S2

## Introduction

This supplementary material presents a brief description of the employed methods, the layout of the experimental device, microscopy images of the used grains, additional graphics, and movies showing examples of interactions of bidisperse barchans. For the latter, we present top view movies for barchans consisting of (i) bidisperse mixtures of grains (file

---

caseb.gif) and (ii) different monodisperse grains (one type for each barchan, file caseo.gif).

We note that complete tables, individual images and movies used in the manuscript are available on Mendeley Data (<http://dx.doi.org/10.17632/sbjtzbzh9k>).

## Methods

### *Preparation of experiments*

The solid particles used in the experiments were glass spheres (see microscopy images in Figs. S2 to S4 below) with diameters  $0.15 \text{ mm} \leq d_{s1} \leq 0.25 \text{ mm}$  and  $0.40 \text{ mm} \leq d_{s2} \leq 0.60 \text{ mm}$  (from Sigmund Lindner company). Prior to each test, they were separated and weighted with a precision scale with a resolution of 0.01 g in order to assure the right proportions of grains forming each initial pile, as well as the total mass of the initial pile. Once weighted, the samples were placed manually in the test section of the channel, already filled with water. With the piles placed on the bottom wall of the channel, a controlled flow of water was imposed and the piles deformed into two barchan dunes that interacted with each other. The desired water flow was fixed manually through globe valves, and the volumetric flow rate was measured with an electromagnetic flow meter (KROHNE, model Optiflux 2010C, 0.5 % uncertainty, maximum measurement capacity of 20 m<sup>3</sup>/h). A Nikon D7500 camera (which has maximum resolution of 1980 px  $\times$  1080 px at 60 Hz) with a lens of 18-140 mm focal distance and F2.8 maximum aperture was mounted on a traveling system and had a top view of the bedforms. The focus was adjusted manually and the pixel to millimeter conversion was carried out by placing a scale in the channel (filled with water) and acquiring a calibration image. In order to obtain the necessary light while avoiding beating with the camera frequency, two lamps of light-emitting diode (LED) with 100W each were used.

### *Image processing*

Once the test run was concluded, the corresponding video file was cropped into frames that were saved as single image files by using functions existing in the Matlab software.

Because of the timescales involved, we processed images corresponding to every 1 s in all tests. The image processing began by converting RGB images in grayscale, and then, using a threshold adjusted manually, into binary images. In order to remove small objects and noise, Matlab built-in filters were used (namely the `medfilt2` and `bwareaopen` functions). After that, some morphological information of identified objects, such as the area, width, length, and centroid positions, were obtained with the built-in function `regionprops`. Properties related to the interacting barchans, such as their width, total length, length of horns, instantaneous separation, etc., were computed with scripts written by ourselves. The process just described was performed inside a loop, which reads and stores the data of every processed image in vectors that are saved in mat files. Finally, mat files are post-processed in order to obtain time evolution of areas, lengths, celerities, etc.

## Captions

**Movie S1.** `caseb.gif` Movie showing an exchange pattern for barchans consisting of bidisperse mixtures (case  $b$  in the main paper).

**Movie S2.** `caseo.gif` Movie showing a collision for barchans consisting of different monodisperse grains (one type for each barchan, case  $o$  in the main paper: the larger upstream barchan reaches the smaller downstream one).

## Figures

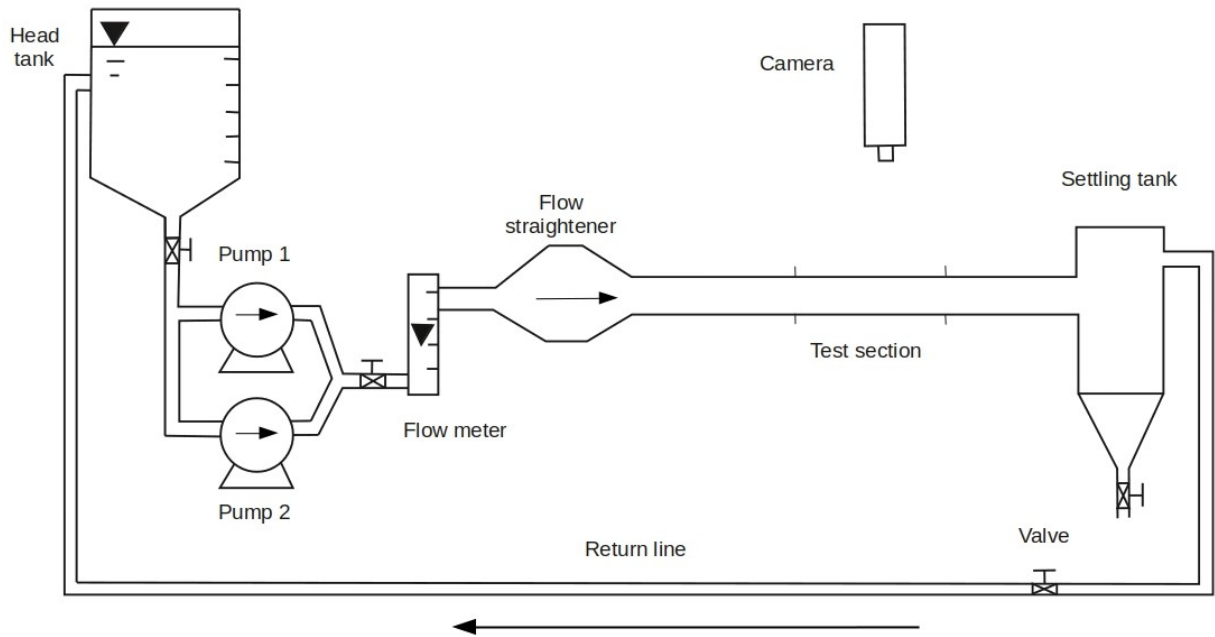


**Figure S1.** Layout of the experimental setup.

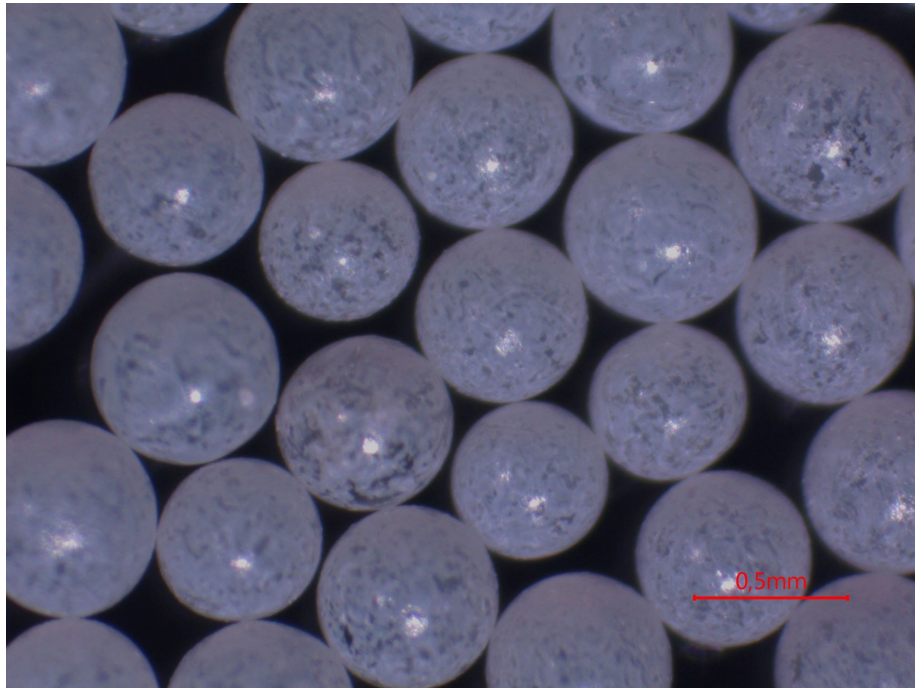


**Figure S2.** Microscopy image for the  $0.40 \text{ mm} \leq d \leq 0.60 \text{ mm}$  round glass beads of white color (species 2).

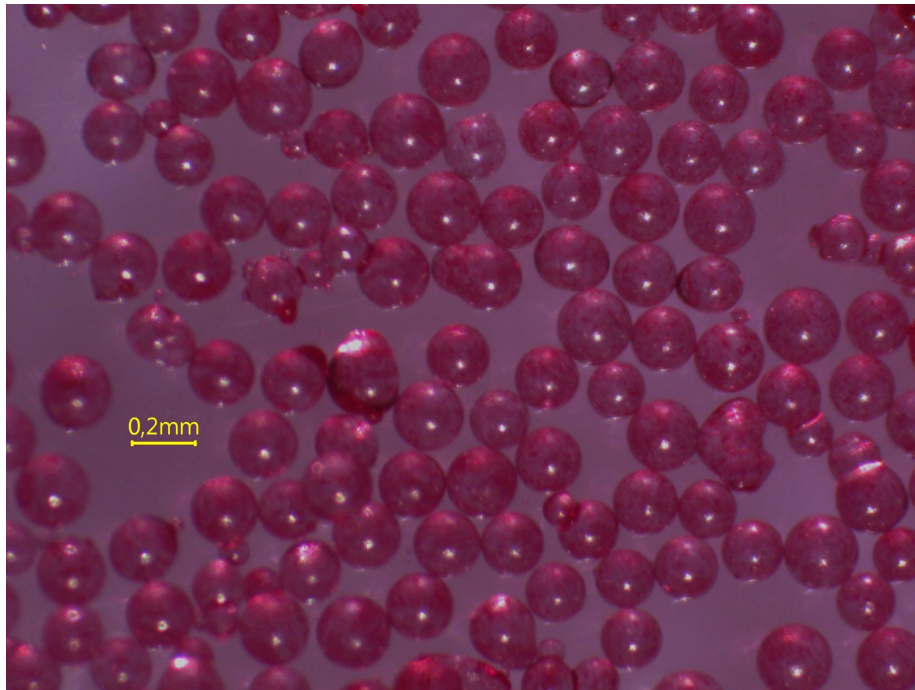


**Figure S3.** Microscopy image for the  $0.15 \text{ mm} \leq d \leq 0.25 \text{ mm}$  round glass beads of red color (species 1).

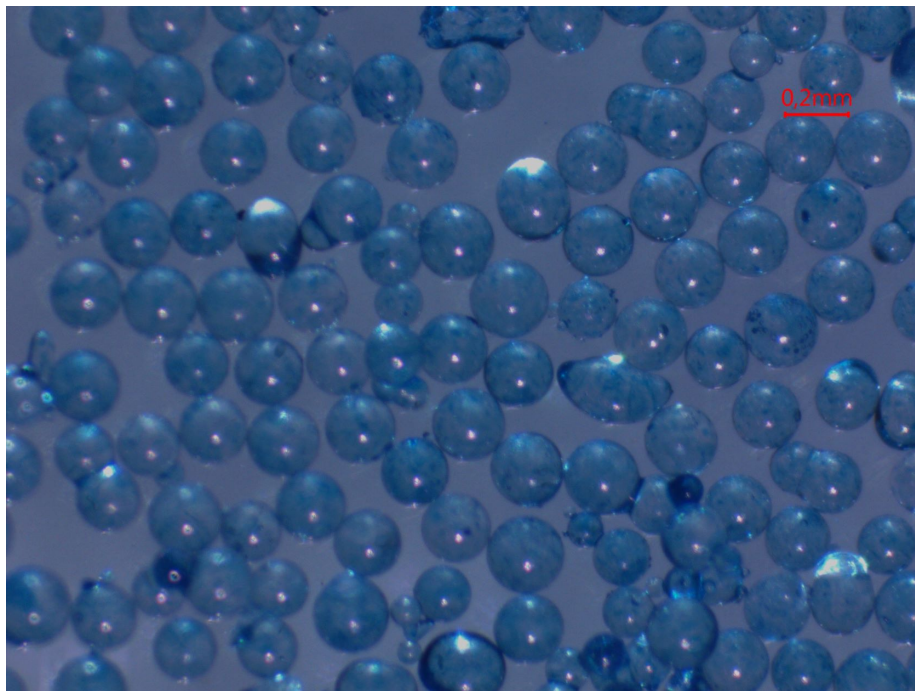


**Figure S4.** Microscopy image for the  $0.15 \text{ mm} \leq d \leq 0.25 \text{ mm}$  round glass beads of blue color (species 1).

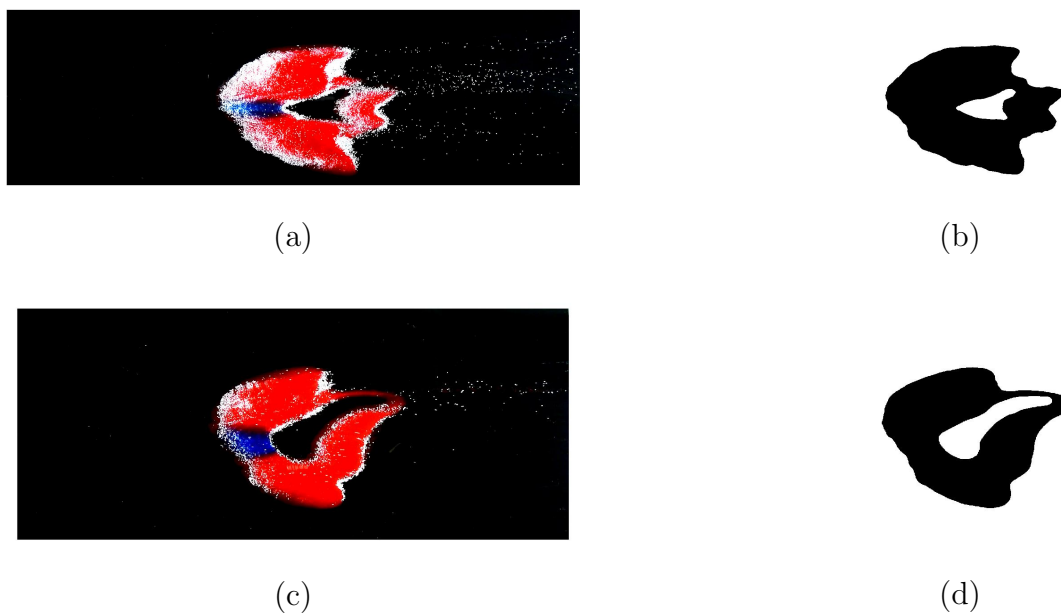


**Figure S5.** Void regions during the exchange processes for (a) and (b)  $\phi_1 = \phi_2 = 0.5$  and (c) and (d)  $\phi_1 \neq \phi_2$ . Figures (a) and (c) are raw images and figures (b) and (d) binarized images.

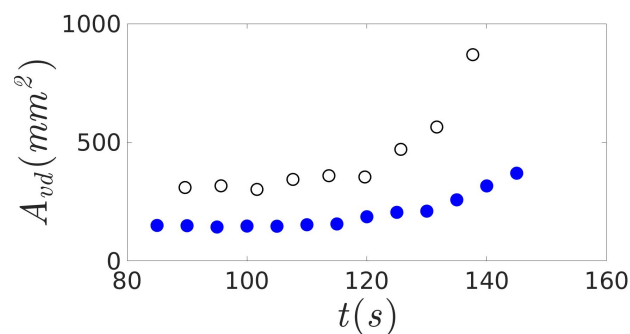


**Figure S6.** Area occupied by the void region  $A_{vd}$  as a function of time, in dimensional form, for the case of bidisperse piles (mixtures). Solid blue circles correspond to the exchange pattern when  $\phi_1 = \phi_2 = 0.5$  and open black symbols when  $\phi_1 \neq \phi_2$ .

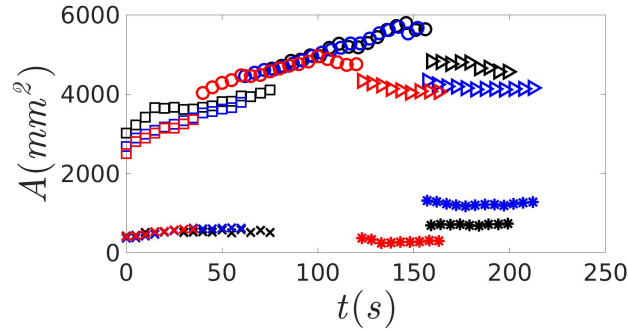


**Figure S7.** Projected areas, in dimensional form, of impact (x), target ( $\square$ ), merged ( $\circ$ ), parent ( $\triangleright$ ) and baby barchans ( $*$ ), respectively, as functions of time, for exchange processes with bidisperse piles (mixtures). Black, blue and red colors correspond to cases  $a$ ,  $f$  and  $h$ .

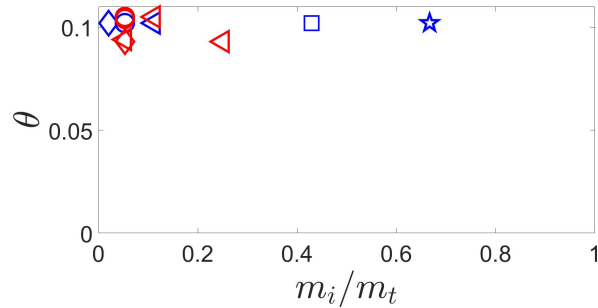


**Figure S8.** Interaction patterns for barchans of bidisperse mixtures in the  $m_i/m_t - \theta$  space: chasing ( $*$ ), merging ( $\diamond$ ), exchange ( $\circ$ ), fragmentation-chasing ( $\square$ ), and fragmentation-exchange ( $\triangleleft$ ). Blue color corresponds to  $\phi_1 = \phi_2 = 0.5$  and red to  $\phi_1 \neq \phi_2$ . We observe that many of the symbols are superposed even if measured patterns are different, since the mass ratio does not take into consideration details about granular compositions.